HHS Public Access

Author manuscript

Mol Cancer Ther. Author manuscript; available in PMC 2024 May 01.

Published in final edited form as:

Mol Cancer Ther. 2023 November 01; 22(11): 1332–1342. doi:10.1158/1535-7163.MCT-22-0804.

Use of Payload Binding Selectivity Enhancers to Improve Therapeutic Index of Maytansinoid-Antibody-Drug Conjugates

Toan D. Nguyen[1], **Brandon M. Bordeau**[1], **Joseph P. Balthasar**[1,*]

[1]Department of Pharmaceutical Sciences, School of Pharmacy and Pharmaceutical Sciences, University at Buffalo, Buffalo, NY 14214

Abstract

Systemic exposure to released cytotoxic payload contributes to the dose-limiting off-target toxicities of anti-cancer antibody-drug conjugates (ADC). In this work, we present an "inverse targeting" strategy to optimize the therapeutic selectivity of maytansinoid-conjugated ADCs. Several anti-maytansinoid sdAbs were generated via phage-display technology with binding IC50s between 10–60 nM. Co-incubation of DM4 with the anti-maytansinoid sdAbs shifted the IC50 of DM4 up to 250-fold. Tolerability and efficacy of 7E7-DM4 ADC, an anti-CD123 DM4-conjugated ADC, were assessed in healthy and in tumor-bearing mice, with and without co-administration of an anti-DM4 sdAb. Co-administration with anti-DM4 sdAb reduced 7E7-DM4 induced-weight loss, where the mean values of percentage weight loss at nadir for mice receiving ADC+saline and ADC+sdAb were 7.9±3% and 3.8±1.3% ($p<0.05$). In tumor-bearing mice, co-administration of the anti-maytansinoid sdAb did not negatively affect the efficacy of 7E7-DM4 on tumor growth or survival following dosing of the ADC at 1 mg/kg ($p=0.49$) or at 10 mg/kg ($p = 0.9$). Administration of 7E7-DM4 at 100 mg/kg led to dramatic weight loss, with 80% of treated mice succumbing to toxicity prior to the appearance of mortality relating to tumor growth in control mice. However, all mice receiving co-dosing of 100 mg/kg 7E7-DM4 with anti-DM4 sdAb were able to tolerate the treatment, which enabled reduction in tumor volume to undetectable levels and to dramatic improvements in survival. In summary, we have demonstrated the utility and feasibility of the application of anti-payload antibody fragments for inverse targeting to improve the selectivity and efficacy of anti-cancer ADC therapy.

Keywords

Antibody-drug Conjugate; Acute Myeloid Leukemia; Maytansinoid; CD123; Antibody; Inverse-targeting

[*]**Corresponding author:** Joseph P. Balthasar, 452 Pharmacy Building, Department of Pharmaceutical Sciences, School of Pharmacy and Pharmaceutical Sciences, University at Buffalo, Buffalo, NY 14214, jb@buffalo.edu, Telphone: 716-645-4807.

Additional Information

Author Contributions: Conceptualization: T.D.N. and J.P.B.; Methodology: T.D.N. and B.M.B.; investigation: T.D.N.; Writing - original draft preparation: T.D.N.; Writing - review and editing: T.D.N. and J.P.B.; Funding acquisition: J.P.B.; Resources: J.P.B.; Supervision: J.P.B.

INTRODUCTION

The major limitation of traditional chemotherapy, excessive systemic toxicity caused by drug exposure in healthy tissue, remains as a limitation for ADC therapy [1–3]. There are two primary mechanisms of payload entry into cells: antigen-mediated endocytosis of ADC-conjugated payloads and passive diffusion of deconjugated payloads. As demonstrated in Figure 1A, ADCs bind to the target antigen and are internalized by receptor-mediated endocytosis. ADCs are subsequently catabolized within the endo-lysosomal system, releasing unconjugated (i.e., “free”) payload molecules that diffuse into the cytoplasm and exert cytotoxic effects. Lysed cancer cells eventually release the unconjugated payloads back into the systemic circulation. Additionally, catabolism of ADCs within non-targeted tissues, or extracellular hydrolysis of the chemical linker that tethers payload to the targeting antibody, yields unconjugated payload that may gain entry into interstitial fluid and plasma, where free payload may diffuse across plasma membranes of healthy, non-targeted cells and subsequently cause undesired, off-site toxicity. Evidence suggests that antigen-mediated endocytosis is the dominant mechanism for uptake of payload into targeted cells, and that passive diffusion of the free payload across the plasma membranes of non-targeted cells is the primary driver of unwanted toxicity [4, 5]. Our lab has proposed that payload-binding molecules may be co-administered with ADCs to bind and “neutralize” released payload in extracellular fluids, blocking distribution of payload into non-targeted cells, as shown in Figure 1B. Payload-binding molecules may be hydrophilic macromolecules, which are designated as payload binding selectivity enhancers (PBSEs), based on our hypothesis that these agents will increase the therapeutic selectivity of ADC therapy.

The inverse targeting concept introduced by Balthasar and Fung theorizes that the therapeutic window of a drug could be improved by decreasing drug distribution to sites associated with drug toxicities [6–8]. Initial work on this strategy considered optimization of regional chemotherapy for cancers confined within a physiological compartment (e.g., intraperitoneal (IP) chemotherapy for treatment of stage II-III ovarian cancer). IP chemotherapy is dose-limited by systemic toxicities that arise due to the distribution of drug from the peritoneum into the blood circulation, and due to subsequent distribution from blood into systemic tissues (e.g., bone marrow) associated with toxicity (e.g., neutropenia). In the inverse targeting strategy of Balthasar and Fung, intravenous (IV) administration of anti-drug antibodies was employed to bind (i.e., intercept) drug within plasma, decreasing the rate and extent of drug distribution to sites associated with toxicity, and enabling increases in the maximum tolerated dose (MTD) and efficacy of IP chemotherapy [8]. Previous studies in the Balthasar laboratory demonstrated that IV co-administration of an anti-methotrexate antigen-binding Fab fragments led to a 5-fold increase in the MTD of IP methotrexate, thus improving the median survival time of mice bearing peritoneal tumors [9]. Similarly, co-dosing of an anti-topotecan antibody IV reduced topotecan-induced weight loss in mice by ~50% [10]. The Balthasar laboratory has proposed that the “inverse targeting” concept may be employed to optimize the therapeutic selectivity of ADC therapy, where anti-payload antibodies may be used to decrease off-target toxicities relating to systemic exposure to released (i.e., “free”) payload. Recently, we reported the development of a humanized anti-MMAE antibody fragment (ABC3315) that increased the therapeutic

index of MMAE based ADCs [11]. ABC3315 ameliorated markers of off-target toxicity in mice that were treated with polatuzumab vedotin (body-weight loss) or trastuzumab-vc-MMAE (bone marrow suppression). In contrast, ABC3315 did not alter the efficacy of polatuzumab vedotin or trastuzumab-vc-MMAE in mouse xenograft models of human cancer.

DM1 and DM4 are potent tubulin-binding maytansinoid payloads utilized in ADC technology [12–14]. In preclinical models, maytansinoid ADCs have shown impressive anti-tumor effects [14–16]. Yet, during clinical trials, treatment with maytansinoid ADCs has yielded only limited efficacy at their MTDs [17, 18]. We hypothesize that dose-limiting toxicities relating to systemic exposure to free DM1 and DM4 may be minimized through administration of anti-DM1/DM4 antibodies, enabling administration of higher doses of DM1/DM4 ADCs, and leading to increased efficacy. This work details the development of anti-CD123-DM4 ADCs and anti-maytansinoid sdAbs. Through a series of in vitro and in vivo studies we demonstrate that the anti-maytansinoid sdAbs may be employed in an "inverse targeting" strategy to increase the therapeutic window of DM4 based ADCs.

METHODS

Pharmacokinetic modeling

A pharmacokinetic model was used to describe the clinical pharmacokinetic data of anetumab ravtansine as a model DM4-ADC. Plasma pharmacokinetic data after intravenous administration of anetumab ravtansine in patients at a dose of 6.5 mg/kg were reported by Hassan et al. [19]. Figure S1 describes the schematics of the plasma pharmacokinetic model for anetumab ravtansine and its metabolites. The pharmacokinetic profile of anetumab ravtansine is captured by a two-compartment pharmacokinetic model with linear clearance (CL_{ADC}) from the central compartment and distributional clearance (CLD_{ADC}) to the peripheral compartment. Degradation of each molecule of the ADC is assumed to form unconjugated payload DM4 in a quantity dictated by the drug-antibody ratio (DAR). Released DM4 is metabolized to form S-methyl-DM4, an active metabolite, via $CL_{metabolism}$. S-Methyl-DM4 is eliminated via a linear clearance pathway, CL_{SMeDM4}. Non-compartmental methods were performed using SimBiology in Matlab software (Mathworks, Natick, MA) to calculate initial estimates of parameters prior to model fittings. Simultaneous fitting of parameters to plasma concentration data was conducted with ADAPT 5 software (Biomedical Simulations Resource, Los Angeles, CA), with listing of fitted parameters in Table S1.

The ADC pharmacokinetic model was merged with another two-compartment model that describes the pharmacokinetics of an anti-maytansinoid sdAb as depicted in Figure 2A. The binding of the sdAb to conjugated DM4, free DM4 payload, and the metabolite S-methyl-DM4 was described with microconstants of binding association (k_{on}) and binding dissociation (k_{off}). The model assumes that: (1) degradation of sdAb-bound ADC contributes to the release of DM4 into the central (plasma containing) compartment, and (2) sdAb-bound DM4 and S-methyl-DM4 have limited distribution and are subject to elimination via the kidney in the same manner as the unbound sdAb. Pharmacokinetic parameters for sdAb were obtained from the literature and were used for the anti-

maytansinoid sdAb [20], and the fitted pharmacokinetic parameters from clinical data of anetumab ravtansine were used for the DM4-ADC. All simulations were conducted in Berkley-Madonna software (University of California at Berkeley, CA), in which ADC and anti-DM4 sdAb were administered as IV infusion doses of 6.5 mg/kg and 2.25 mg/kg (1:1 ratio of sdAb to conjugated DM4) over one hour. Subsequently, an additional 9 doses of anti-DM4 sdAb were simulated via IP dosing every 6 hours. The IP absorption rate constant (k_a) was set at 0.5 h^{-1}. The final set of model equations employed to predict the impact of anti-maytansinoid sdAb on DM4-ADC pharmacokinetics are:

ADC PK

$$\frac{dC1_{ADC}}{dt} = \frac{CLD_{ADC} \times C2_{ADC}}{V1_{ADC}} - \frac{CLD_{ADC} \times C1_{ADC}}{V1_{ADC}} - \frac{CL_{ADC} \times C1_{ADC}}{V1_{ADC}} - k_{on} \times C1_{ADC} \times C1_{sdAb} + k_{off} \times Cb1_{ADC}$$

$$\frac{dC2_{ADC}}{dt} = -\frac{CLD_{ADC} \times C2_{ADC}}{V2_{ADC}} - \frac{CLD_{ADC} \times C1_{ADC}}{V2_{ADC}}$$

SdAb-bound ADC PK

$$\frac{dCb1_{ADC}}{dt} = \frac{CLD_{ADC} \times Cb2_{ADC}}{V1_{ADC}} - \frac{CLD_{ADC} \times Cb1_{ADC}}{V1_{ADC}} - \frac{CL_{ADC} \times Cb1_{ADC}}{V1_{ADC}} + k_{on} \times C1_{ADC} \times C1_{sdAb} - k_{off} \times Cb1_{ADC}$$

$$\frac{dCb2_{ADC}}{dt} = -\frac{CLD_{ADC} \times Cb2_{ADC}}{V2_{ADC}} - \frac{CLD_{ADC} \times Cb1_{ADC}}{V2_{ADC}}$$

Anti-maytansinoid sdAb PK

$$\frac{dC1_{sdAb}}{dt} = \frac{CLD_{sdAb} \times C2_{sdAb}}{V1_{sdAb}} - \frac{CLD_{sdAb} \times C1_{sdAb}}{V1_{sdAb}} - \frac{CL_{sdAb} \times C1_{sdAb}}{V1_{sdAb}} - k_{on} \times C1_{ADC} \times C1_{sdAb} + k_{off} \times Cb1_{ADC} - k_{on} \times C_{DM4} \times C1_{sdAb} + k_{off} \times Cb_{DM4} - k_{on} \times C_{SMeDM4} \times C1_{sdAb} + k_{off} \times Cb_{SMeDM4} - \frac{GFR \times C1\_sdAb}{V1_{sdAb}}$$

$$\frac{dC2_{sdAb}}{dt} = -\frac{CLD_{sdAb} \times C1_{sdAb}}{V2_{sdAb}} - \frac{CLD_{sdAb} \times C2_{sdAb}}{V2_{sdAb}}$$

DM4 PK

$$\frac{dC_{DM4}}{dt} = \frac{CL_{ADC} \times DAR \times (C1_{ADC} + Cb1_{ADC})}{V_{DM4}} - \frac{CL_{met} \times C_{DM4}}{V_{DM4}} - k_{on} \times C_{DM4} \times C1_{sdAb} \times \frac{V1_{sdAb}}{V_{DM4}} + k_{off} \times Cb_{DM4} \times \frac{V1_{sdAb}}{V_{DM4}}$$

$$\frac{dCb_{DM4}}{dt} = k_{on} \times C_{DM4} \times C1_{sdAb} - k_{off} \times Cb_{DM4} - \frac{GFR \times Cb_{DM4}}{V1_{sdAb}}$$

S-methyl-DM4 PK

$$\frac{dC_{SMeDM4}}{dt} = \frac{CL_{met} \times C_{DM4}}{V_{DM4}} - \frac{CL_{SMeDM4} \times C_{SMeDM4}}{V_{DM4}} - k_{on} \times C_{SMeDM4} \times C1_{sdAb} \times \frac{V1_{sdAb}}{V_{DM4}} + k_{off} \times Cb_{SMeDM4} \times \frac{V1_{sdAb}}{V_{DM4}}$$

$$\frac{dCb_{SMeDM4}}{dt} = k_{on} \times C_{SMeDM4} \times C1_{sdAb} - k_{off} \times Cb_{SMeDM4} - \frac{GFR \times Cb_{SMeDM4}}{V1_{sdAb}}$$

Generation of anti-CD123 DM4-ADCs

Development of anti-CD123 mAbs are detailed in supplementary methods. Anti-CD123 mAbs, 7E7 and 11C3, and a control non-targeting mAb 8C2 (an anti-topotecan antibody previously developed in our lab [21]), were used to develop ADCs with DM4 via the N-succinimidyl-4-(2-pyridyldithio) butyrate (SPDB) cleavable linker. Briefly, anti-CD123 mAbs (5 mg/mL) were buffer exchanged into HEPES buffer pH 8.0. To this solution, SPDB-DM4 linker-payload (MedChemExpress, Monmouth Junction, NJ), 10 mM in DMSO, was added at a molar ratio of 10:1 drug to antibody, and the mixture was incubated for 18 hours at room temperature before buffer exchange and dialysis into PBS. ADCs were stored at 4°C prior to use. The concentrations of linked DM4 and antibody components in the conjugate were estimated by the formula:

$$[\mathrm{DM4}] = [\mathrm{A}_{252\mathrm{nm}} - (\mathrm{A}_{280\mathrm{nm}} \cdot (\varepsilon^{\mathrm{Ab}}{}_{250\mathrm{nm}}/\varepsilon^{\mathrm{Ab}}{}_{280\mathrm{nm}}))]/[\varepsilon^{\mathrm{DM4}}{}_{252\mathrm{nm}} - (\varepsilon^{\mathrm{DM4}}{}_{280\mathrm{nm}} \cdot (\varepsilon^{\mathrm{Ab}}{}_{252\mathrm{nm}}/\varepsilon^{\mathrm{Ab}}{}_{280\mathrm{nm}})]$$

$$[\mathrm{Ab}] = \left[\mathrm{A}_{280\mathrm{nm}} - \left(\mathrm{A}_{252\mathrm{nm}} \cdot \left(\varepsilon^{\mathrm{DM4}}{}_{280\mathrm{nm}}/\varepsilon^{\mathrm{DM4}}{}_{252\mathrm{nm}}\right)\right)\right]/\left[\varepsilon^{\mathrm{Ab}}{}_{280\mathrm{nm}} - \left(\varepsilon^{\mathrm{Ab}}{}_{252\mathrm{nm}} \cdot \left(\varepsilon^{\mathrm{DM4}}{}_{280\mathrm{nm}}/\varepsilon^{\mathrm{DM4}}{}_{252\mathrm{nm}}\right)\right)\right]$$

The values of extinction coefficients used are [13]:

$$\varepsilon^{\mathrm{Ab}}{}_{280\mathrm{nm}} = 223,000\mathrm{M}^{-1}\mathrm{cm}^{-1}; \varepsilon^{\mathrm{Ab}}{}_{252\mathrm{nm}} = 82,510\mathrm{M}^{-1}\mathrm{cm}^{-1}$$
$$\varepsilon^{\mathrm{DM4}}{}_{280\mathrm{nm}} = 5180\mathrm{M}^{-1}\mathrm{cm}^{-1}; \varepsilon^{\mathrm{DM4}}{}_{252\mathrm{nm}} = 26,160\mathrm{M}^{-1}\mathrm{cm}^{-1}$$

Development of anti-maytansinoid sdAbs

Immunization and library construction—DM4 was conjugated to maleimide-activated mariculture keyhole limpet hemocyanin (KLH) (Thermo Fisher Scientific, Rockford, IL) following the manufacturer's protocol. A llama (Capralogics, Hardwick, MA) was subcutaneously immunized with 300 μg of KLH-DM4 in incomplete Freund's adjuvant every three weeks for a total of four immunizations. Ten days after the fourth immunization, 600 mL of freshly harvested blood was used to isolate peripheral blood lymphocytes, and total RNA was extracted from the lymphocytes using TRizol reagents. Llama sdAb

phage display libraries were built using the extracted RNAs as previously described with modifications [22].

Phage panning to enrich anti-DM1/DM4 sdAb binders—DM1 and DM4 were conjugated to Biotin-Maleimide and used for bio-panning and screening of anti-maytansinoid sdAbs. Briefly, 200 μg of Biotin-Maleimide was conjugated with 740 μg of DM1/DM4 in 1 mL phosphate-buffered saline (PBS) pH 7.0. The reaction was incubated overnight at room temperature and stored at 4°C until use. Stock streptavidin magnetic beads (Thermo Fisher Scientific, Rockford, IL) were washed three times with PBS + 0.05% Tween 20 (PBST) and blocked with PBS + 5% non-fat dry milk (MPBS) for 2 h. After the blocking step, the streptavidin beads were incubated with 1 mL of 1 μM biotin-DM1/DM4 for 15 minutes, followed by three washes with PBST. For the first panning input, the stock phage was diluted to 10^{12} c.f.u. (colony forming unit)/mL in blocking buffer (2% milk PBS), and 1 ml of the diluted phage was distributed into each well and incubated for 2 hours. After the incubation, beads were washed with PBST 5 times, 10 times, 15 times, and 15 times for the 1st, 2nd, 3rd, and 4th round of panning. Bound phages were then eluted either by incubation with 500 μL of 1 mg/ml trypsin for 30 min or by incubation with free DM1 or DM4 solution at the concentrations of 1 μM, 100 nM, 10 nM, and 1 nM in PBS over 1 hour for the 1st, 2nd, 3rd, and 4th round of panning. Output phages were titrated and re-infected with TG-1 cells for phage production in the next round of panning.

Screening of anti-DM1/DM4 single domain antibodies—Phage-infected TG1 cells were grown overnight, serially diluted in 2xYT media, spread over individual culture plates containing selective medium (LB agar + 100 μg/mL ampicillin + 2% wt/v glucose), and incubated overnight at 37°C. A master plate was generated by inoculating a single colony into wells of a 96-well round-bottom culture plate filled with 100 μL of 2xYT supplemented with 100 μg/mL ampicillin, 2% (wt/vol) glucose, and 15% (vol/vol) glycerol, and grown overnight at 37°C, 300 rpm. These wells were then used to inoculate wells of 96 deep-well plates containing 1 mL of 2xYT medium (100 μg/mL ampicillin per well). Plates were incubated for 4 h at 37°C and 300 rpm until OD600 ≈ 0.5, then 1 μL of stock helper phage was added to each well and incubated for another 1 hour. Kanamycin was added to a final concentration of 50 μg/mL, and the plates were incubated overnight at 30°C 250 rpm.

Nunc Maxisorp 96-well ELISA plates were coated with 4 μg/ml NeutrAvidin (Thermo Fisher Scientific, Rockford, IL) overnight at 4°C. Plates were washed five times with PBST, and blocked with MPBS for 2 h at RT, then100 μL of 1 μM Biotin-DM1/DM4 was added for 30 minutes. Plates were then washed five times with PBST and incubated with 4-fold diluted phage supernatant for 2 h, with or without pre-incubation of free DM1/DM4 at a concentration range from 10 nM to 10 μM. Plates were then washed five times with PBST, and bound sdAb-displaying phages were detected using an anti-M13 phage HRP-conjugated antibody (Antibody Design Labs, San Diego, CA) diluted 1:1000 in MPBS for 1-hour. Following five washes with PBST, 100 μL of 1-Step Turbo TMB-ELISA solution was added to each well and incubated for 15 minutes. The reaction was quenched by adding 100 μL of Stop solution (Thermo Fisher Scientific, Rockford, IL) to each well, and absorbance was measured at 450 nm.

Affinity maturation of the anti-DM4 sdAbs—Random mutations were introduced into the original anti-maytansinoid sdAbs through error-prone PCR [23]. PCR primers were designed to facilitate the error-prone PCR products to be transferred from pET-22b expression vector for protein expression into pComb3XSS phagemid vector for library construction, and vice versa.

Bio-panning was performed to identify high-affinity binders targeting DM4. In summary, stock StrepAvidin magnetic beads were blocked with 2% milk PBST for 1 hour at room temperature; then, the blocked beads were incubated with 500 μL of biotin-DM4 for 30 minutes before the phage binding step. Approximately 10^{12} phages in PBST were incubated with the avidin-biotin-DM4 beads for another 1 hour, then washed and eluted via a free-drug competition method or an off-rate method [24]. For the free-drug competition method, bound phages were incubated for 1 hour with 500 μL of 10 nM, 1 nM, and 0.1 nM DM4 in PBS in the first, second, and third round of panning, then the supernatant was collected and used for the subsequent round of panning or screening. For the off-rate method, bound phages were incubated with 1 mL of 1 μM DM4 in PBS overnight at 4°C, then on the next day, the supernatant was discarded, and the remaining bound phages were eluted with trypsin. One hundred clones from the third round of each panning method were screened with phage media. Twenty positive clones from each screening that had the highest binding signal to avidin-biotin-DM1/DM4 were rescreened via a competitive assay with DM4. Briefly, phage media was diluted 4-fold in PBST containing free DM4 at the final concentrations of 100 nM, 50 nM, or 10 nM, and incubated for 1-hour before the antigen-binding step of ELISA. The newly identified derivative clones were assessed for affinity toward free DM4 via competitive ELISA, and anti-DM4 antagonism with cell cytotoxicity assays. Expression and purification of the sdAbs were detailed in supplemental methods.

In vitro cell cytotoxicity assay

Log-phase SK-BR-3 cells (HTB-30, ATCC, Manassas, VA, RRID: CVCL_0033) were seeded in 96-well microtiter plates at a density of 5,000 cells/well, in 100 μL culture medium. Cells were allowed to adhere for 24 h before cell culture media was aspirated and replaced with culture media containing treatments, followed by a 96-hour incubation at 37°C. Treatment solutions for SK-BR-3 cells consist of DM4 or S-methyl-DM4 over a concentration range of 0.1–1000 nM, with and without 10 μM of anti-maytansinoid sdAb. After the treatment period, treatment media was aspirated, and cells were washed three times with 100 μL of fresh media. Following the final wash, 100 μL of complete media and 25 μL of 3-(4,5-Dimethylthiazol-2-yl)-2,5-Diphenyltetrazolium Bromide (MTT) solution were added to each well. Cells were incubated for 4 h to allow cells to reduce MTT to formazan dye. Once MTT was reduced, 100 μL of 10% SDS prepared in 0.01 M HCl was added to each well and incubated overnight to solubilize the formazan crystals. Formazan dye was measured at 570 nm and normalized by cell debris at 640 nm. The SK-BR-3 cells were not authenticated or tested for Mycoplasma contamination.

In vivo tolerability investigations

The effect of co-administration of anti-maytansinoid sdAb on the toxicity of DM4-ADC was determined in healthy mice (Swiss Webster, Taconic). Body weight loss was used as the toxicodynamic biomarker. On day 0, three groups of mice (n = 6) were given a single IV dose of either vehicle control or 55 mg/kg of 7E7-DM4. Immediately after the injection, the control group, the ADC+PBS group, and the ADC+PBSE group were injected IP with PBS, PBS, and anti-maytansinoid sdAb, respectively, every 6 hours over 10 injections. For the ADC+PBSE group, the molar ratio of each sdAb dose and the conjugated DM4 was 1. The body weights of the mice were measured daily for up to 13 days. Mean % bodyweight vs. time plot was generated for each group, where the percentage body weight for each animal was calculated based on their body weight on day 0. The animals were monitored daily for signs of toxicity, including bodyweight loss, dehydration, hunched posture, ruffled fur, and loss of appetite or lethargy. The protocols of animal experiments detailed in this manuscript had been approved by the University at Buffalo Institutional Animal Care and Use Committee.

In vivo efficacy study

An AML xenograft model was established by injecting 6-week-old male Nu/J mice (The Jackson Laboratory, RRID:IMSR_JAX:002019) in the right flank with 5 million MOLM-14 cells (DSMZ, Braunschweig, Germany, RRID:CVCL_7916) in 200 μl of RPMI media. Once tumor volumes reached 100–250 mm^3, mice were split into seven groups of treatments (n = 5 animals/group): PBS vehicle control, 1 mg/kg of ADC+PBS, 1 mg/kg ADC+PBSE, 10 mg/kg of ADC+PBS, 10 mg/kg of ADC+PBSE, 100 mg/kg of ADC+PBS, and 100 mg/kg of ADC+PBSE. PBS vehicle control or 7E7-DM4 ADC was given IV. Immediately after the injection, the control group, the ADC+PBS group, and the ADC+PBSE group were injected IV with PBS, PBS, and anti-maytansinoid PBSE, respectively, and followed up with IP injections every 6 hours over 9 injections. For the ADC+PBSE group, the molar ratio of each PBSE dose to the conjugated DM4 was around 1:1. Tumor size was measured every day using digital calipers with tumor volume calculated using the formula: tumor volume = ($Width^2$ x Length)/2. Kaplan–Meier survival curves were generated in GraphPad Prism 7 and compared using the log-rank test at a significance level of $P \leq 0.005$.

Data availability

The data generated in this study are available upon request from the corresponding author.

RESULTS

PK/PD modeling and simulation

Clinical pharmacokinetic data for anetumab ravtansine, a mesothelin-targeting DM4-ADC, and its metabolites were fitted with a two-compartment pharmacokinetic model (Figure S1). All parameter estimates are reported in Table S1. Using the estimated pharmacokinetic parameters of anetumab ravtansine and sdAb pharmacokinetic parameters from a published study [20], the pharmacokinetics of DM4-ADC were simulated with and without co-administration of an anti-maytansinoid sdAb. As demonstrated in Figure 2B, the model

predicts that co-administration of the anti-maytansinoid sdAb with the same molar ratio as conjugated DM4 would significantly reduce the systemic concentration of unconjugated DM4 and S-methyl-DM4. In addition to the concentration profile, simulated AUCs also indicate that co-administration of anti-maytansinoid sdAb significantly decreases cumulative systemic exposures of DM4 and S-methyl-DM4 by 46% and 61%, respectively (Figure 2C).

Generation of anti-CD123 DM4-ADCs

High-affinity anti-CD123 mAbs were developed via hybridoma technology. Figure S2 presents the surface plasmon resonance (SPR) sensorgrams obtained by passing different concentrations of anti-CD123 mAbs over a sensor chip immobilized with recombinant human CD123. SPR analyses indicate that both 7E7 and 11C3 mAbs bind to the immobilized CD123 with high affinity, and their binding dissociation constants (Kd) were estimated to be 88 pM and 55 pM, respectively. 7E7 and 11C3 DM4-ADCs were generated using a cleavable disulfide linker SPDB, and drug-to-antibody ratios (DAR) were estimated to be 3.8 to 4 through the UV absorbance method. Figure S3 shows the binding curves for the anti-CD123 mAbs and ADCs to MOLM-14 AML cells. Both 7E7 and 11C3 mAbs exhibit high binding affinity toward the cellular CD123 target, and their fitted IC50 values are 2.26 and 2.39 nM, respectively. Both 7E7 and 11C3 ADCs demonstrated comparable binding affinity to their parent mAbs with the fitted IC50 values of 2.63 and 6.01 nM, respectively.

A panel of AML cell lines was treated with CD123-targeting and non-targeting ADCs for 96 hours, followed by an MTT-based assay to assess cell cytotoxicity. The results were normalized to cells treated with vehicle control and reported as % cell viability. Both anti-CD123 ADCs, 7E7-DM4 and 11C3-DM4, displayed potent cytotoxicity with IC50 values between 1 to 10 nM in an antigen-dependent manner (Figure S4 and Table S2). Cell lines with high expression of CD123, i.e., MOLM-14 and MV-4-11, are more responsive to 7E7 and 11C3 than cell lines with moderate or low expression, i.e., KG-1 and Kasumi-3. In the AML cell line with no expression of CD123 (Namalwa), the cytotoxicities of both targeting and non-targeting ADCs were comparable.

Anti-maytansinoid sdAbs development

Several sdAbs specific to maytansinoids were generated via phage-display technology, and random mutagenesis was performed to generate constructs with improved selectivity and affinity. The affinity of the anti-DM4 sdAbs was determined by competitive ELISA with free DM4. As demonstrated in Figure 3A, all clones isolated from the mutated library have moderate to high affinity to free DM4 with KD values ranging from 10 nM to 56 nM. The estimated affinities are also in line with the initial screening and cytotoxicity assay, as DMFH1 and DMOH9 were identified as the two clones with the highest affinity values. Table S3 summarizes the characteristics of the lead derivative clones. Activity of the anti-DM4 sdAbs, in terms of antagonizing DM4-induced cytotoxicity, was evaluated with use of SK-BR-3 cells and the MTT assay. The IC50 of DM4 in SK-BR-3 cells was between 0.3 to 0.4 nM. In the presence of 10 μM of purified anti-DM4 sdAbs, DM4 cytotoxicity was reduced up to 250-fold to an IC50 of ~100 nM (Figure 3B).

Figure 4A demonstrates binding activity of the lead anti-DM4 sdAbs DMOH9 and DMFH1 to the active metabolite S-methyl-DM4, with the binding IC50 values of 14.9 and 19.4 nM, respectively. Additionally, in the presence of purified anti-DM4 sdAbs, DMFH1 and DMOH9, S-methyl-DM4 cytotoxicity was reduced more than 100-fold from IC50s of less than 30 pM to 3.93 nM and 4.10 nM, respectively (Figure 4B).

In vivo tolerability

The effects of anti-maytansinoid PBSE on the tolerability of the 7E7-DM4 ADC were evaluated in healthy Swiss-Webster mice. A single IV dose of 7E7-DM4 was well tolerated at doses up to 45 mg/kg with only minimal change in body weight. The mice experienced more substantial toxicity at higher doses, with the % nadir weight loss observed at 55mg/kg dose being 10.8±1.14% (Figure S5). Co-dosing of PBSE (Figure 5A) reduced ADC-related toxicity, with the %nadir weight loss of the ADC+PBS and ADC+PBSE groups being 7.9 ± 3% and 3.8 ± 1.3% (P=0.023), respectively (Figure 5B).

In vivo efficacy

The effect of anti-maytansinoid PBSE on the efficacy of anti-CD123-DM4 ADC was evaluated in an AML xenograft animal model. MOLM-14 tumor-bearing mice were treated with either vehicle control, 1 mg/kg, 10 mg/kg, or 100 mg/kg 7E7-DM4 with or without PBSE. The resulting tumor growth and survival curves are shown in Figure 5C and 5D, respectively. The ADC was active at the low dose of 1 mg/kg, significantly prolonged survival from the control group (P = 0.002). At the 10 mg/kg dose, the ADC substantially suppressed tumor growth and significantly improved survival relative to the 1 mg/kg dose group (P = 0.0021) and the control group (P = 0.001). Co-administration of the anti-maytansinoid PBSE did not significantly affect tumor growth and survival for following 1 mg/kg dosing (P = 0.49) or 10 mg/kg dosing (P = 0.9). At the dose of 100 mg/kg of ADC, the treated mice experienced significant toxicity, and 80% of the animals were euthanized by day 7 post treatment due to body weight loss ≥20%. Strikingly, all of the mice treated with 100 mg/kg of ADC with PBSE were found to tolerate treatment, with complete tumor regression observed in all treated mice, and with no tumor growth observed for 75-days post-ADC dosing.

DISCUSSION

Traditional drug targeting strategies aim to improve therapeutic selectivity by directing drugs to desired sites of drug activity, thus increasing the efficiency of drug delivery to the tumor. On the other hand, inverse targeting seeks to enhance therapeutic selectivity by decreasing drug delivery to healthy tissues [8, 10]. Given that exposure to released payload is a likely contributor to ADC toxicity [1–3], we proposed using payload-binding antibody fragments within an inverse targeting strategy to improve the therapeutic selectivity of ADCs. The objectives of our approach are (1) to reduce the systemic free payload exposure, (2) to decrease ADC-related systemic toxicity, (3) to enable increases in the maximum tolerated dose of ADCs, and ultimately (4) to enhance the therapeutic efficacy of ADCs in the treatment of cancer.

Maytansine is a tubulin-binding agent that shows potent anti-tumor activity in pre-clinical animal models; however, its clinical development was terminated due to unacceptable toxicities in patients [25]. With recent advances in ADC technology, interest in maytansine was revived and maytansine-derivatives such as DM1 and DM4 have been extensively evaluated as cytotoxic ADC payloads. Trastuzumab emtansine, T-DM1, has been FDA-approved for treatment of breast cancer, and many additional ADCs utilizing maytansinoid payloads have been developed. However, many maytansinoid-based ADCs have been discontinued in late stages of clinical investigation due to suboptimal responses at the maximum tolerated doses (MTDs) [1, 26, 27].

Data from multiple clinical trials investigating DM4-ADC pharmacokinetics have shown that the plasma concentrations of free DM4 and its active metabolite, S-methyl-DM4 (SMe-DM4), achieve values that are several-fold higher than their cytotoxic concentrations (as determined in cell culture experiments). For instance, in a phase II clinical trial of indatuximab ravtansine (anti-CD138-DM4 with SPDB cleavable linker) for treatment of multiple myeloma, mean plasma concentrations of DM4 in patients treated at the MTD of 140 mg/m^2 were in the range of 5.0–21.9 ng/mL (6.3–27.6 nM) during the treatment period [28, 29]. Similarly, free payload plasma concentrations in patients were detected in the range of 1 to 100 nM for additional DM4-ADCs such as AVE9633 (anti-CD33-SPDB-DM4 for treatment of acute myeloid leukemia) [30] and coltuximab ravtansine (anti-CD19-SPDB-DM4 for treatment of B-cell lymphoma) [14, 17, 31]. Considering that the IC50 values of DM4 and SMe-DM4 are in the picomolar range when applied to most cell lines [12, 13, 32], these plasma concentrations of free DM4 and SMe-DM4 in patients are 10–1000 fold higher than their active concentrations. These observations suggest that the free payload may be the primary driver of the off-target toxicity associated with DM4-ADC treatments. Off-target toxicities define the MTD of ADC therapies and, ultimately, the doses used in clinical trials and in clinical practice [3].

Single domain antibodies are antibody fragments derived from variable domains of “heavy-chain only” IgG2 and IgG3 antibodies that are naturally expressed by members of the Camelidae family [33]. Due to their smaller size and monodomain structure, sdAbs are easier to manipulate genetically, relative to other common antibody fragments such as Fab or scFv [34]. Furthermore, sdAbs are highly homologous to human VHs and are less prone to stability, aggregation, and degradation than Fab or scFvs [34, 35]. Following administration to humans or other mammals, sdAbs are rapidly eliminated via renal filtration due to their small size (about 15 kDa), which is below the glomerular filtration molecular weight cut-off (approximately 60 kDa) [35]. On the other hand, DM1, DM4 and their active metabolites are primarily cleared by hepatic biotransformation and biliary secretion, with a relatively long in vivo half-life of 2 to 8 days [16]. We hypothesize that anti-maytansinoid sdAb may be employed to bind free DM1 and DM4 in the systemic circulation, decreasing distribution to healthy tissues associated with DM1 and DM4 toxicities, and that sdAb-DM1 and sdAb-DM4 complexes will be rapidly eliminated via renal excretion.

Tolerable clinical doses of ADCs are below levels needed to achieve tumor-curative exposures, as defined in preclinical models [36]. Additionally, ADCs typically demonstrate very steep dose-effect and dose-toxicity relationships. For example, in a phase I clinical trial

of sacituzumab govitecan for the treatment of diverse epithelial cancers, a 25% increase in dose from 8 mg/kg to 10 mg/kg led to a significant increase in toxicity with 21% versus 47% of patients experiencing grade 3+ neutropenia [37]. However, this dose increases also led to a substantial increase in efficacy with 36% vs. 64% of patients with partial response or stable disease, for those receiving 8 mg/kg versus 10 mg/kg. We hypothesize that neutralizing free payload in the systemic circulation will decrease ADC off-target toxicity, increasing the maximum tolerated ADC dose, and enabling an improved response to ADC treatment.

Mathematical modeling and simulation were utilized to evaluate the feasibility of the inverse targeting strategy for DM4-ADCs. Studies in mice showed that unconjugated DM4 payload is rapidly converted into the more potent metabolite SMe-DM4 by S-methyl-transferases. Subsequently, the metabolite is S-oxidated into sulfoxide and sulfone metabolites in the liver and eventually eliminated via secretion in the bile [38, 39]. The model assumes one compartment for both DM4 and S-methyl-DM4 with a shared volume of distribution. Since eliminated DM4 payload is predominantly in the S-methylated form, the model assumes that the metabolism clearance of DM4 is the same as the formation clearance of SMe-DM4. Free sdAbs and bound sdAbs to DM4 and SMe-DM4 are expected to be rapidly removed from the systemic circulation via glomerular filtration [20]. Therefore, co-administration of anti-maytansinoid sdAb provides an additional clearance pathway, i.e., renal elimination of sdAb-DM4/DM4 metabolite complexes, enabling a reduction in their cumulative systemic exposure.

It is well appreciated that mice tolerate doses of ADCs and small molecule chemotherapeutics that are much greater than the tolerable doses in humans [36]. The maximum tolerated dose of DM4-ADCs in mice is approximately 55 mg/kg [14, 40]. Similar results were observed in the initial tolerability study of our anti-CD123-DM4 ADC. Mice injected with a single IV dose of the 7E7-DM4 ADC experienced minimal weight loss with doses up to 40 mg/kg, and the maximum tolerated dose was determined to be 55 mg/kg. Co-dosing of 7E7-DM4 with the anti-maytansinoid sdAb PBSE at a 10:1 molar ratio of PBSE:conjugated-DM4 reduced nadir weight loss by ~50%. In addition, the *in vivo* efficacy study demonstrated no significant difference in tumor progression and median survival time among the 1 or 10 mg/kg ADC dose groups with vs. without co-dosing of PBSE. By decreasing off-site toxicity, anti-DM4 PBSE treatment enabled mice to tolerate the 100 mg/kg ADC dose, allowing complete regression of the MOLM-14 xenograft tumors. Of note, our study did not include a negative control PBSE antibody fragment. Although administration of a non-binding fragment is not expected to influence ADC-induced toxicity or anti-tumor activity, negative control PBSE will be included in future work.

Besides toxicities driven by unconjugated payloads, non-specific uptake of intact ADCs in healthy tissues might also contribute to off-target toxicities [5]. For example, hepatotoxicity is one of the significant off-target toxicities associated with DM1- and DM4-ADCs in pre-clinical and clinical studies [41]. Recently, Endo et al. suggested that the cytoskeleton-associated protein 5 (CKAP5) expressed on the hepatocyte cell surface could interact with maytansinoid-based ADCs, leading to plasma membrane disruption and cell apoptosis [42, 43]. This interaction is independent of the antibody target and highly specific

for maytansinoid payloads, including DM1 and DM4. Additionally, ocular toxicity is another dose-limiting clinical adverse event associated with DM4-ADCs and MMAF-ADCs [44]. Data from Zhao et al. suggested that uptake of intact ADCs via nonspecific macropinocytosis by corneal cells might contribute to the ocular toxicity associated with ADC treatments [45]. In addition, they demonstrated that modifying charges or hydrophobicity of the ADCs decreased the nonspecific uptake of ADCs into human corneal epithelial cells *in vitro* and reduced ocular toxicity *in vivo*. The impact of PBSE on the off-target toxicities driven by the uptake of intact ADCs will be pursued in subsequent studies.

The application of inverse targeting for ADCs is a unique strategy for mitigating payload-associated ADC toxicities without requiring alteration of the structure or composition of the ADC; thus, the inverse targeting strategy may be employed to optimize therapy with ADCs that are on the market and in current clinical development. Several approaches have been introduced to limit the off-target toxicity of ADCs, including modifications of either the targeting antibody [46, 47], the linker [16, 48], or the payload itself [13, 49–51]. As all of these approaches require alterations of the structure of ADCs, and because each ADC is unique and may behave differently, these approaches may not be easily translatable from one ADC to another. On the other hand, anti-payload PBSE could be used as an adjuvant to existing ADCs. Even though more than a hundred ADCs are being developed, there are only six classes of payload that make up for more than 95% of ADCs [36, 52, 53]. Therefore, PBSE with affinity for a given payload, or family of payloads, may be applied to optimize therapy with many ADCs.

In addition to anti-cancer efficacy that is driven by antigen-mediated internalization of intact ADC agents, ADCs with cleavable linkers may have additional anti-tumor activity through the bystander effect, where released payload distributes from ADC-targeted cells to neighboring cells and causes cell death. For example, the released payload of MMAE-conjugated ADCs demonstrates a potent bystander effect on antigen-negative cells in *in vitro* co-culture systems [54]. Studies using patient-derived xenograft models treated with MMAE-ADCs indicated that bystander activity is also relevant *in vivo* [55, 56]. Similar observations can be found with maytansinoid-conjugated and PBD-conjugated ADCs [57, 58]. In addition, clinical data from patients treated with brentuximab vedotin, an FDA-approved anti-CD30-MMAE ADC, show no correlation between clinical outcome vs. CD30 expression, suggesting that the bystander effect might provide an essential role in clinical efficacy [59]. For our inverse targeting strategy, evaluating the impact of payload binders on the bystander effect is a primary concern. In this manuscript, our *in vivo* study has shown no negative impact of co-dosing of anti-DM4 PBSE on the efficacy of the 7E7-DM4 ADC in a MOLM-14 xenograft model. We are unaware of a validated bystander xenograft model to allow *in vivo* testing of the effects of PBSE on bystander activity in the context of AML. However, we have recently demonstrated that anti-MMAE PBSE does not negatively impact the efficacy of trastuzumab-vc-MMAE in a “bystander” HER2+/HER-NCI-N87/MCF7 xenograft model, suggesting that our PBSE optimization strategy may be employed without loss of within-tumor bystander activity [11]. In summary, we have demonstrated the utility and feasibility of our inverse targeting strategy for ADCs, where co-dosing of anti-maytansinoid PBSE and maytansinoid-based ADCs enables reduced ADC

toxicity, increases in the ADC MTD, and increases in ADC anti-tumor efficacy. Our initial results will require confirmation in dedicated toxicology studies, and engineering (e.g., for half-life extension) will be needed to enable more convenient PBSE dosing. Optimization of PBSE characteristics and dosing will be pursued in future work and may allow further improvements in ADC selectivity and efficacy.

Supplementary Material

Refer to Web version on PubMed Central for supplementary material.

Acknowledgements:

The authors would like to thank Maureen Adolf for her assistance with hybridoma fusion.

Funding:

Portions of this work were supported by the Center for Protein Therapeutics at the University at Buffalo, and by grants from the National Cancer Institute (CA246785, CA256928, CA275967).

Financial support:

This work was supported by the National Cancer Institute (CA246785, CA256928, CA275967).

Conflict of Interest Disclosure Statement:

J.P.B., B.M.B, and T.D.N. are founders of Abceutics, Inc., which is pursuing development of payload binding agents to enhance the therapeutic selectivity of antibody-drug conjugates. J.P.B, B.M.B., and T.D.N. have financial interest through WO2021113740A1. J.P.B. serves as the Director of the University at Buffalo Center for Protein Therapeutics, which is supported by AbbVie, Amgen, AstraZeneca, CSL-Behring, Eli Lilly, Genentech, GSK, Janssen, Merck, Roche, and Sanofi. During the course of this work, J.P.B. has received consulting fees from companies involved with the development of cancer therapies, including Abbvie, Amgen, Janssen, Eli Lilly, Merck, and Sanofi.

REFERENCES

1. Saber H and Leighton JK (2015) An FDA oncology analysis of antibody-drug conjugates. Regul Toxicol Pharmacol 71:444–52. doi: 10.1016/j.yrtph.2015.01.014 [PubMed: 25661711]
2. Saber H, Simpson N, Ricks TK and Leighton JK (2019) An FDA oncology analysis of toxicities associated with PBD-containing antibody-drug conjugates. Regul Toxicol Pharmacol 107:104429. doi: 10.1016/j.yrtph.2019.104429 [PubMed: 31325532]
3. Masters JC, Nickens DJ, Xuan D, Shazer RL and Amantea M (2018) Clinical toxicity of antibody drug conjugates: a meta-analysis of payloads. Investigational New Drugs 36:121–135. doi: 10.1007/s10637-017-0520-6 [PubMed: 29027591]
4. Colombo R and Rich JR (2022) The therapeutic window of antibody drug conjugates: A dogma in need of revision. Cancer Cell 40:1255–1263. doi: 10.1016/j.ccell.2022.09.016 [PubMed: 36240779]
5. Nguyen TD, Bordeau BM and Balthasar JP (2023) Mechanisms of ADC Toxicity and Strategies to Increase ADC Tolerability. Cancers 15:713. [PubMed: 36765668]
6. Balthasar J and Fung HL (1994) Utilization of antidrug antibody fragments for the optimization of intraperitoneal drug therapy: studies using digoxin as a model drug. J Pharmacol Exp Ther 268:734–9. [PubMed: 8113985]
7. Balthasar JP and Fung HL (1995) High-affinity rabbit antibodies directed against methotrexate: production, purification, characterization, and pharmacokinetics in the rat. J Pharm Sci 84:2–6. doi: 10.1002/jps.2600840103 [PubMed: 7714737]
8. Balthasar JP and Fung HL (1996) Inverse targeting of peritoneal tumors: selective alteration of the disposition of methotrexate through the use of anti-methotrexate antibodies and antibody fragments. J Pharm Sci 85:1035–43. doi: 10.1021/js960135w [PubMed: 8897267]

9. Lobo ED and Balthasar JP (2005) Application of anti-methotrexate Fab fragments for the optimization of intraperitoneal methotrexate therapy in a murine model of peritoneal cancer. J Pharm Sci 94:1957–64. doi: 10.1002/jps.20422 [PubMed: 16052545]
10. Shah DK and Balthasar JP (2014) PK/TD modeling for prediction of the effects of 8C2, an anti-topotecan mAb, on topotecan-induced toxicity in mice. Int J Pharm 465:228–38. doi: 10.1016/j.ijpharm.2014.01.038 [PubMed: 24508555]
11. Bordeau BM, Nguyen TD, Polli JR, Chen P and Balthasar JP (2023) Payload-Binding Fab Fragments Increase the Therapeutic Index of MMAE Antibody–Drug Conjugates. Molecular Cancer Therapeutics 22:459–470. doi: 10.1158/1535-7163.Mct-22-0440 [PubMed: 36723609]
12. Erickson HK, Park PU, Widdison WC, Kovtun YV, Garrett LM, Hoffman K, Lutz RJ, Goldmacher VS and Blättler WA (2006) Antibody-Maytansinoid Conjugates Are Activated in Targeted Cancer Cells by Lysosomal Degradation and Linker-Dependent Intracellular Processing. Cancer Research 66:4426. doi: 10.1158/0008-5472.CAN-05-4489 [PubMed: 16618769]
13. Widdison WC, Wilhelm SD, Cavanagh EE, Whiteman KR, Leece BA, Kovtun Y, Goldmacher VS, Xie H, Steeves RM, Lutz RJ, Zhao R, Wang L, Blättler WA and Chari RVJ (2006) Semisynthetic Maytansine Analogues for the Targeted Treatment of Cancer. Journal of Medicinal Chemistry 49:4392–4408. doi: 10.1021/jm060319f [PubMed: 16821799]
14. Hong EE, Erickson H, Lutz RJ, Whiteman KR, Jones G, Kovtun Y, Blanc V and Lambert JM (2015) Design of Coltuximab Ravtansine, a CD19-Targeting Antibody–Drug Conjugate (ADC) for the Treatment of B-Cell Malignancies: Structure–Activity Relationships and Preclinical Evaluation. Molecular Pharmaceutics 12:1703–1716. doi: 10.1021/acs.molpharmaceut.5b00175 [PubMed: 25856201]
15. Ab O, Whiteman KR, Bartle LM, Sun X, Singh R, Tavares D, LaBelle A, Payne G, Lutz RJ, Pinkas J, Goldmacher VS, Chittenden T and Lambert JM (2015) IMGN853, a Folate Receptor-alpha (FRalpha)-Targeting Antibody-Drug Conjugate, Exhibits Potent Targeted Antitumor Activity against FRalpha-Expressing Tumors. Mol Cancer Ther 14:1605–13. doi: 10.1158/1535-7163.Mct-14-1095 [PubMed: 25904506]
16. Zhao RY, Wilhelm SD, Audette C, Jones G, Leece BA, Lazar AC, Goldmacher VS, Singh R, Kovtun Y, Widdison WC, Lambert JM and Chari RVJ (2011) Synthesis and Evaluation of Hydrophilic Linkers for Antibody–Maytansinoid Conjugates. Journal of Medicinal Chemistry 54:3606–3623. doi: 10.1021/jm2002958 [PubMed: 21517041]
17. Trneny M, Verhoef G, Dyer MJ, Ben Yehuda D, Patti C, Canales M, Lopez A, Awan FT, Montgomery PG, Janikova A, Barbui AM, Sulek K, Terol MJ, Radford J, Guidetti A, Di Nicola M, Siraudin L, Hatteville L, Schwab S, Oprea C and Gianni AM (2018) A phase II multicenter study of the anti-CD19 antibody drug conjugate coltuximab ravtansine (SAR3419) in patients with relapsed or refractory diffuse large B-cell lymphoma previously treated with rituximab-based immunotherapy. Haematologica 103:1351–1358. doi: 10.3324/haematol.2017.168401 [PubMed: 29748443]
18. Coiffier B, Thieblemont C, Guibert S, Dupuis J, Ribrag V, Bouabdallah R, Morschhauser F, Navarro R, Gouill SL, Haioun C, Houot R, Casasnovas O, Holte H, Lamy T, Broussais F, Payrard S, Hatteville L and Tilly H (2016) A phase II, single-arm, multicentre study of coltuximab ravtansine (SAR3419) and rituximab in patients with relapsed or refractory diffuse large B-cell lymphoma. British Journal of Haematology 173:722–730. doi: 10.1111/bjh.13992 [PubMed: 27010483]
19. Hassan R, Blumenschein GR Jr., Moore KN, Santin AD, Kindler HL, Nemunaitis JJ, Seward SM, Thomas A, Kim SK, Rajagopalan P, Walter AO, Laurent D, Childs BH, Sarapa N, Elbi C and Bendell JC (2020) First-in-Human, Multicenter, Phase I Dose-Escalation and Expansion Study of Anti-Mesothelin Antibody-Drug Conjugate Anetumab Ravtansine in Advanced or Metastatic Solid Tumors. J Clin Oncol:Jco1902085. doi: 10.1200/jco.19.02085
20. Hoefman S, Ottevaere I, Baumeister J and Sargentini-Maier ML (2015) Pre-Clinical Intravenous Serum Pharmacokinetics of Albumin Binding and Non-Half-Life Extended Nanobodies®. Antibodies 4:141–156.
21. Shah DK and Balthasar JP (2014) Predicting the effects of 8C2, a monoclonal anti-topotecan antibody, on plasma and tissue disposition of topotecan. J Pharmacokinet Pharmacodyn 41:55–69. doi: 10.1007/s10928-013-9346-9 [PubMed: 24368689]

22. Alvarez-Rueda N, Behar G, Ferre V, Pugniere M, Roquet F, Gastinel L, Jacquot C, Aubry J, Baty D, Barbet J and Birkle S (2007) Generation of llama single-domain antibodies against methotrexate, a prototypical hapten. Mol Immunol 44:1680–90. doi: 10.1016/j.molimm.2006.08.007 [PubMed: 17011035]
23. McCullum EO, Williams BAR, Zhang J and Chaput JC (2010) Random Mutagenesis by Error-Prone PCR. Humana Press, pp. 103–109
24. Pírez-Schirmer M, Rossotti M, Badagian N, Leizagoyen C, Brena BM and González-Sapienza G (2017) Comparison of Three Antihapten VHH Selection Strategies for the Development of Highly Sensitive Immunoassays for Microcystins. Analytical Chemistry 89:6800–6806. doi: 10.1021/acs.analchem.7b01221 [PubMed: 28494149]
25. Issell BF and Crooke ST (1978) Maytansine. Cancer Treatment Reviews 5:199–207. doi: 10.1016/S0305-7372(78)80014-0 [PubMed: 367597]
26. Donaghy H (2016) Effects of antibody, drug and linker on the preclinical and clinical toxicities of antibody-drug conjugates. MAbs 8:659–71. doi: 10.1080/19420862.2016.1156829 [PubMed: 27045800]
27. Joubert N, Denevault-Sabourin C, Bryden F and Viaud-Massuard MC (2017) Towards antibody-drug conjugates and prodrug strategies with extracellular stimuli-responsive drug delivery in the tumor microenvironment for cancer therapy. European Journal Of Medicinal Chemistry 142:393–415. doi: 10.1016/j.ejmech.2017.08.049 [PubMed: 28911823]
28. Ikeda H, Hideshima T, Fulciniti M, Lutz RJ, Yasui H, Okawa Y, Kiziltepe T, Vallet S, Pozzi S, Santo L, Perrone G, Tai Y-T, Cirstea D, Raje NS, Uherek C, Dälken B, Aigner S, Osterroth F, Munshi N, Richardson P and Anderson KC (2009) The Monoclonal Antibody nBT062 Conjugated to Cytotoxic Maytansinoids Has Selective Cytotoxicity Against CD138-Positive Multiple Myeloma Cells In vitro and In vivo</em&gt. Clinical Cancer Research 15:4028. doi: 10.1158/1078-0432.CCR-08-2867 [PubMed: 19509164]
29. Jagannath S, Heffner LT, Ailawadhi S, Munshi NC, Zimmerman TM, Rosenblatt J, Lonial S, Chanan-Khan A, Ruehle M, Rharbaoui F, Haeder T, Wartenberg-Demand A and Anderson KC (2019) Indatuximab Ravtansine (BT062) Monotherapy in Patients With Relapsed and/or Refractory Multiple Myeloma. Clinical Lymphoma Myeloma and Leukemia 19:372–380. doi: 10.1016/j.clml.2019.02.006
30. Lapusan S, Vidriales MB, Thomas X, de Botton S, Vekhoff A, Tang R, Dumontet C, Morariu-Zamfir R, Lambert JM, Ozoux M-L, Poncelet P, San Miguel JF, Legrand O, DeAngelo DJ, Giles FJ and Marie J-P (2012) Phase I studies of AVE9633, an anti-CD33 antibody-maytansinoid conjugate, in adult patients with relapsed/refractory acute myeloid leukemia. Investigational New Drugs 30:1121–1131. doi: 10.1007/s10637-011-9670-0 [PubMed: 21519855]
31. Carol H, Szymanska B, Evans K, Boehm I, Houghton PJ, Smith MA and Lock RB (2013) The anti-CD19 antibody-drug conjugate SAR3419 prevents hematolymphoid relapse postinduction therapy in preclinical models of pediatric acute lymphoblastic leukemia. Clin Cancer Res 19:1795–805. doi: 10.1158/1078-0432.Ccr-12-3613 [PubMed: 23426279]
32. Lopus M, Oroudjev E, Wilson L, Wilhelm S, Widdison W, Chari R and Jordan MA (2010) Maytansine and Cellular Metabolites of Antibody-Maytansinoid Conjugates Strongly Suppress Microtubule Dynamics by Binding to Microtubules. Molecular Cancer Therapeutics 9:2689. doi: 10.1158/1535-7163.MCT-10-0644 [PubMed: 20937594]
33. Arbabi Ghahroudi M, Desmyter A, Wyns L, Hamers R and Muyldermans S (1997) Selection and identification of single domain antibody fragments from camel heavy-chain antibodies. FEBS Letters 414:521–526. doi: 10.1016/S0014-5793(97)01062-4 [PubMed: 9323027]
34. Muyldermans S (2001) Single domain camel antibodies: current status. Reviews in Molecular Biotechnology 74:277–302. doi: 10.1016/S1389-0352(01)00021-6 [PubMed: 11526908]
35. Harmsen MM and De Haard HJ (2007) Properties, production, and applications of camelid single-domain antibody fragments. Appl Microbiol Biotechnol 77:13–22. doi: 10.1007/s00253-007-1142-2 [PubMed: 17704915]
36. de Goeij BE and Lambert JM (2016) New developments for antibody-drug conjugate-based therapeutic approaches. Curr Opin Immunol 40:14–23. doi: 10.1016/j.coi.2016.02.008 [PubMed: 26963132]

37. Ocean AJ, Starodub AN, Bardia A, Vahdat LT, Isakoff SJ, Guarino M, Messersmith WA, Picozzi VJ, Mayer IA, Wegener WA, Maliakal P, Govindan SV, Sharkey RM and Goldenberg DM (2017) Sacituzumab govitecan (IMMU-132), an anti-Trop-2-SN-38 antibody-drug conjugate for the treatment of diverse epithelial cancers: Safety and pharmacokinetics. Cancer 123:3843–3854. doi: 10.1002/cncr.30789 [PubMed: 28558150]
38. Sun X, Widdison W, Mayo M, Wilhelm S, Leece B, Chari R, Singh R and Erickson H (2011) Design of Antibody−Maytansinoid Conjugates Allows for Efficient Detoxification via Liver Metabolism. Bioconjugate Chemistry 22:728–735. doi: 10.1021/bc100498q [PubMed: 21391620]
39. Erickson HK and Lambert JM (2012) ADME of antibody-maytansinoid conjugates. Aaps j 14:799–805. doi: 10.1208/s12248-012-9386-x [PubMed: 22875610]
40. Sun X, Ponte JF, Yoder NC, Laleau R, Coccia J, Lanieri L, Qiu Q, Wu R, Hong E, Bogalhas M, Wang L, Dong L, Setiady Y, Maloney EK, Ab O, Zhang X, Pinkas J, Keating TA, Chari R, Erickson HK and Lambert JM (2017) Effects of Drug–Antibody Ratio on Pharmacokinetics, Biodistribution, Efficacy, and Tolerability of Antibody–Maytansinoid Conjugates. Bioconjugate Chemistry 28:1371–1381. doi: 10.1021/acs.bioconjchem.7b00062 [PubMed: 28388844]
41. Taplin S, Vashisht K, Walles M, Calise D, Kluwe W, Bouchard P and Johnson R (2018) Hepatotoxicity with antibody maytansinoid conjugates: A review of preclinical and clinical findings. J Appl Toxicol 38:600–615. doi: 10.1002/jat.3582 [PubMed: 29388692]
42. Endo Y, Takeda K, Mohan N, Shen Y, Jiang J, Rotstein D and Wu WJ (2018) Payload of T-DM1 binds to cell surface cytoskeleton-associated protein 5 to mediate cytotoxicity of hepatocytes. Oncotarget 9:37200–37215. doi: 10.18632/oncotarget.26461 [PubMed: 30647854]
43. Endo Y, Mohan N, Dokmanovic M and Wu WJ (2021) Mechanisms contributing to ado-trastuzumab emtansine-induced toxicities: a gateway to better understanding of ADC-associated toxicities. Antibody Therapeutics 4:55–59. doi: 10.1093/abt/tbab005 [PubMed: 33937626]
44. (2015) Ocular Adverse Events Associated with Antibody–Drug Conjugates in Human Clinical Trials. Journal of Ocular Pharmacology and Therapeutics 31:589–604. doi: 10.1089/jop.2015.0064 [PubMed: 26539624]
45. Zhao H, Atkinson J, Gulesserian S, Zeng Z, Nater J, Ou J, Yang P, Morrison K, Coleman J, Malik F, Challita-Eid P, Karki S, Aviña H, Hubert R, Capo L, Snyder J, Moon S-J, Luethy R, Mendelsohn BA, Stover DR and Doñate F (2018) Modulation of Macropinocytosis-Mediated Internalization Decreases Ocular Toxicity of Antibody–Drug Conjugates. Cancer Research 78:2115–2126. doi: 10.1158/0008-5472.can-17-3202 [PubMed: 29382707]
46. Zhou Q (2017) Site-Specific Antibody Conjugation for ADC and Beyond. Biomedicines 5. doi: 10.3390/biomedicines5040064
47. Polu KR and Lowman HB (2014) Probody therapeutics for targeting antibodies to diseased tissue. Expert Opinion on Biological Therapy 14:1049–1053. doi: 10.1517/14712598.2014.920814 [PubMed: 24845630]
48. Pillow TH, Schutten M, Yu SF, Ohri R, Sadowsky J, Poon KA, Solis W, Zhong F, Del Rosario G, Go MAT, Lau J, Yee S, He J, Liu L, Ng C, Xu K, Leipold DD, Kamath AV, Zhang D, Masterson L, Gregson SJ, Howard PW, Fang F, Chen J, Gunzner-Toste J, Kozak KK, Spencer S, Polakis P, Polson AG, Flygare JA and Junutula JR (2017) Modulating Therapeutic Activity and Toxicity of Pyrrolobenzodiazepine Antibody-Drug Conjugates with Self-Immolative Disulfide Linkers. Mol Cancer Ther 16:871–878. doi: 10.1158/1535-7163.Mct-16-0641 [PubMed: 28223423]
49. Miller ML, Fishkin NE, Li W, Whiteman KR, Kovtun Y, Reid EE, Archer KE, Maloney EK, Audette CA, Mayo MF, Wilhelm A, Modafferi HA, Singh R, Pinkas J, Goldmacher V, Lambert JM and Chari RV (2016) A New Class of Antibody-Drug Conjugates with Potent DNA Alkylating Activity. Mol Cancer Ther 15:1870–8. doi: 10.1158/1535-7163.Mct-16-0184 [PubMed: 27216304]
50. Miller ML, Shizuka M, Wilhelm A, Salomon P, Reid EE, Lanieri L, Sikka S, Maloney EK, Harvey L, Qiu Q, Archer KE, Bai C, Vitharana D, Harris L, Singh R, Ponte JF, Yoder NC, Kovtun Y, Lai KC, Ab O, Pinkas J, Keating TA and Chari RVJ (2018) A DNA-Interacting Payload Designed to Eliminate Cross-Linking Improves the Therapeutic Index of Antibody–Drug Conjugates (ADCs). Molecular Cancer Therapeutics 17:650. doi: 10.1158/1535-7163.MCT-17-0940 [PubMed: 29440292]

51. Mantaj J, Jackson PJ, Rahman KM and Thurston DE (2017) From Anthramycin to Pyrrolobenzodiazepine (PBD)-Containing Antibody-Drug Conjugates (ADCs). Angew Chem Int Ed Engl 56:462–488. doi: 10.1002/anie.201510610 [PubMed: 27862776]
52. Amani N, Dorkoosh FA and Mobedi H (2020) ADCs, as Novel Revolutionary Weapons for Providing a Step Forward in Targeted Therapy of Malignancies. Curr Drug Deliv 17:23–51. doi: 10.2174/1567201816666191121145109 [PubMed: 31755387]
53. Khongorzul P, Ling CJ, Khan FU, Ihsan AU and Zhang J (2020) Antibody–Drug Conjugates: A Comprehensive Review. Molecular Cancer Research 18:3. doi: 10.1158/1541-7786.MCR-19-0582 [PubMed: 31659006]
54. Singh AP, Sharma S and Shah DK (2016) Quantitative characterization of in vitro bystander effect of antibody-drug conjugates. J Pharmacokinet Pharmacodyn 43:567–582. doi: 10.1007/s10928-016-9495-8 [PubMed: 27670282]
55. Breij ECW, De Goeij BECG, Verploegen S, Schuurhuis DH, Amirkhosravi A, Francis J, Miller VB, Houtkamp M, Bleeker WK, Satijn D and Parren PWHI(2014) An Antibody–Drug Conjugate That Targets Tissue Factor Exhibits Potent Therapeutic Activity against a Broad Range of Solid Tumors. Cancer Research 74:1214–1226. doi: 10.1158/0008-5472.can-13-2440 [PubMed: 24371232]
56. Li F, Emmerton KK, Jonas M, Zhang X, Miyamoto JB, Setter JR, Nicholas ND, Okeley NM, Lyon RP, Benjamin DR and Law C-L (2016) Intracellular Released Payload Influences Potency and Bystander-Killing Effects of Antibody-Drug Conjugates in Preclinical Models. Cancer Research 76:2710–2719. doi: 10.1158/0008-5472.can-15-1795 [PubMed: 26921341]
57. Kovtun YV, Audette CA, Ye Y, Xie H, Ruberti MF, Phinney SJ, Leece BA, Chittenden T, Blättler WA and Goldmacher VS (2006) Antibody-Drug Conjugates Designed to Eradicate Tumors with Homogeneous and Heterogeneous Expression of the Target Antigen. Cancer Research 66:3214. doi: 10.1158/0008-5472.CAN-05-3973 [PubMed: 16540673]
58. Zammarchi F, Corbett S, Adams L, Tyrer PC, Kiakos K, Janghra N, Marafioti T, Britten CE, Havenith CEG, Chivers S, D'Hooge F, Williams DG, Tiberghien A, Howard PW, Hartley JA and Van Berkel PH (2018) ADCT-402, a PBD dimer–containing antibody drug conjugate targeting CD19-expressing malignancies. Blood 131:1094–1105. doi: 10.1182/blood-2017-10-813493 [PubMed: 29298756]
59. Staudacher AH and Brown MP (2017) Antibody drug conjugates and bystander killing: is antigen-dependent internalisation required? British Journal of Cancer 117:1736–1742. doi: 10.1038/bjc.2017.367 [PubMed: 29065110]

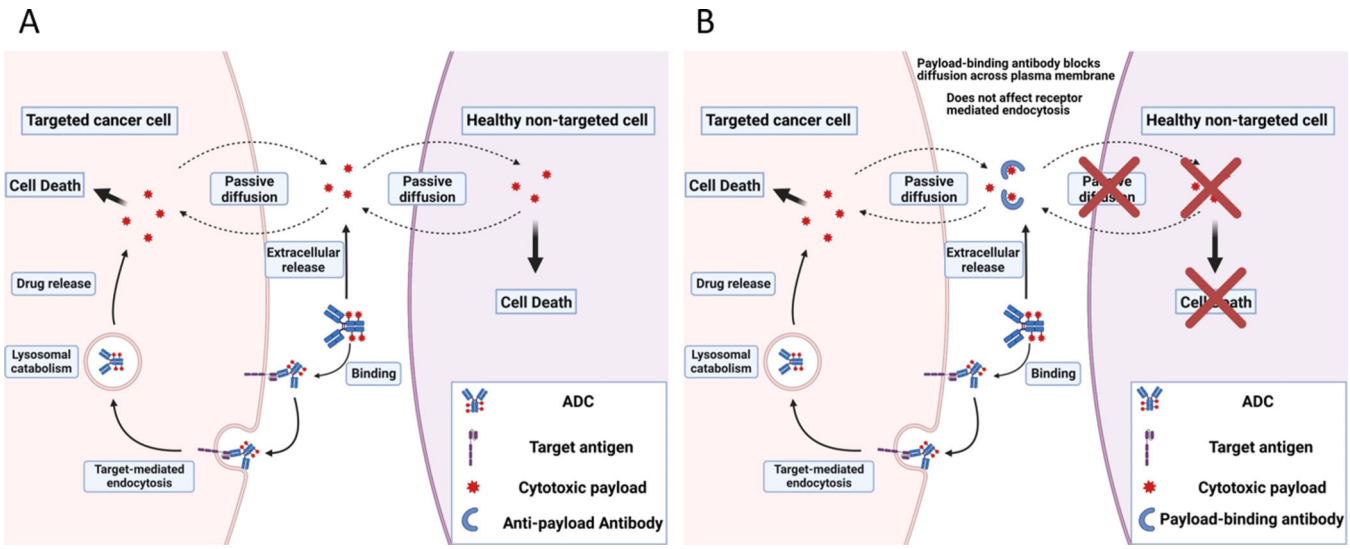

Figure 1. Inverse targeting strategy to reduce ADC toxicity associated with free payload.

(A) Major uptake mechanisms for ADCs and cytotoxic payloads. ADCs are internalized into targeted cells by receptor mediated endocytosis, and the drug linker is catabolized within the lysosomal space releasing the payload. Free payload can diffuse out of targeted cells, or cells that non-specifically degrade ADC, and into untargeted healthy cells resulting in off-target toxicities. **(B)** Proposed "inverse targeting" strategy to block off-target toxicity related to free payload exposure. Payload-binding agents (e.g., single domain antibodies, sdAb) bind and "neutralize" released payload in extracellular fluid (e.g., plasma), blocking diffusion of released payload across plasma membranes of untargeted cells, while not interfering with the receptor-mediated endocytosis of ADCs by targeted cancer cells.

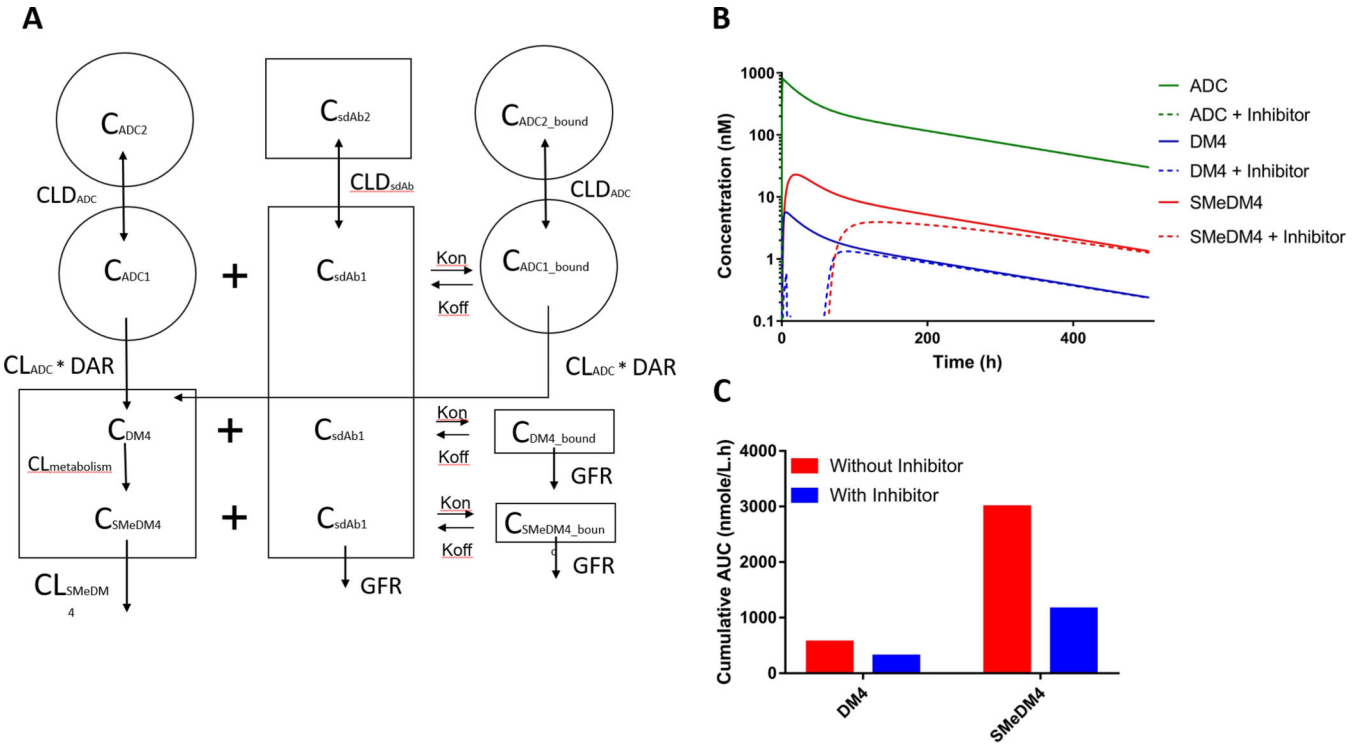

Figure 2. Simulations to predict the impact of anti-maytansonoid single-domain antibodies (sdAb) on DM4 and S-methy DM4 pharmacokinetics following ADC dosing.

(A) A two-compartment model was used to simulate the plasma pharmacokinetics of anti-DM4 sdAb. Binding of the sdAb to conjugated DM4, free DM4 payload, and the metabolite S-methyl-DM4 was described with k_{on} and k_{off} rate constants. A complete description of the model structure is provided in the methods section. **(B)** Model simulation of ADC and free payload plasma concentrations with or without co-administration of an anti-maytansinoid sdAb (inhibitor). The model predicts that co-administration of the anti-maytansinoid sdAb at a ten-fold molar ratio relative to DM4 significantly reduces the plasma concentrations of unconjugated DM4 and S-methyl-DM4. **(C)** Impact of anti-DM4 sdAb on the area under the DM4 and S-methyl-DM4 plasma concentration vs. time curves (AUCs). Co-administration of anti-maytansinoid sdAb is predicted to decrease DM4 and S-methyl-DM4 plasma AUCs by 46% and 61%, respectively.

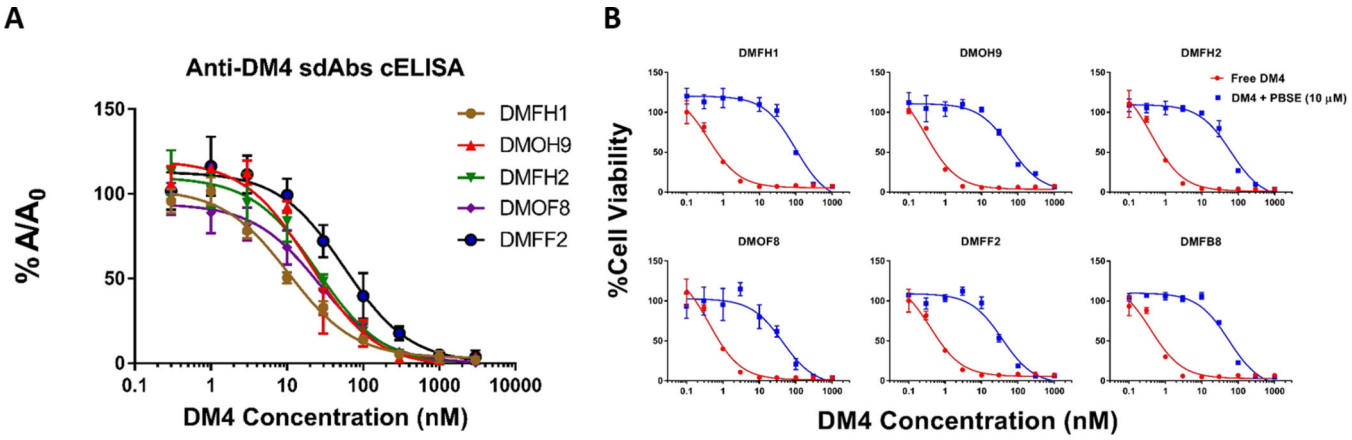

Figure 3. Binding evaluation of the anti-maytansinoid sdAbs to DM4.

(A) Affinity characterization of the derivative anti-maytansinoid single-domain antibodies (sdAb) to free DM4. Binding activity of the sdAbs against free DM4 was evaluated via competitive enzyme linked immunosorbent assay (ELISA). The concentration of each anti-DM4 sdAb was held constant, and free DM4 at concentrations ranging from 0.1 nM to 1 μM were added. Solutions were incubated for 30 minutes before being added to an ELISA plate coated with DM4-biotin-avidin. The fraction bound (%A/A_0) of the sdAbs to immobilized DM4 decreased with increasing concentrations of free DM4. Points represent the mean of samples in triplicate with standard deviations depicted by the error bars. All clones isolated from the mutated library have moderate to high affinity to free DM4, with IC50 values ranging from 10 nM to 56 nM. The calculated binding IC50s are reported in Table S3. **(B)** Anti-maytansinoid sdAbs potently inhibit DM4 cytotoxicity. SK-BR-3 cells were incubated with DM4 (100 pM – 1000 nM) with or without co-incubation with 10 μM of purified anti-maytansinoid sdAb over a 24 h exposure period, following with viability assay to assess cell cytotoxicity. The results were normalized to cells treated with vehicle control and reported as % cell viability. The data was fitted for cytotoxic IC50 values with Hill slope in GraphPad Prism software. Each data point represents the mean of triplicate samples with standard deviations shown with error bars. The IC50 of DM4 applied to SK-BR-3 cells was between 0.3 to 0.4 nM. In the presence of 10 μM of purified anti-DM4 sdAbs, DM4 cytotoxicity was reduced up to 250-fold. Calculated IC50s are reported in Table S3.

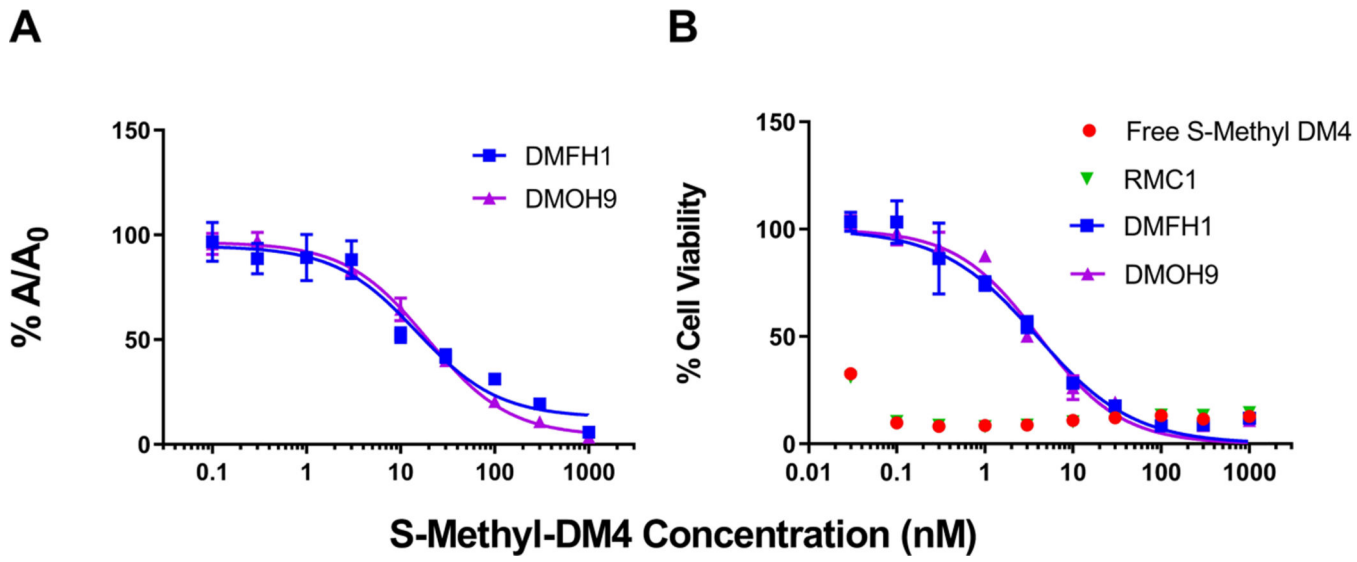

Figure 4. Binding evaluation of the anti-maytansinoid sdAbs to S-methyl-DM4.

(A) Affinity assessment of the sdAbs against S-methyl-DM4 was evaluated via competitive enzyme linked immunosorbent assay (ELISA). The concentration of each anti-DM4 sdAb was held constant, and free S-methyl-DM4 at concentrations ranging from 0.1 nM to 1 μM were added. Solutions were incubated for 30 minutes before being added to an ELISA plate coated with DM4-biotin-avidin. The fraction bound (%A/A_0) of the sdAbs to immobilized DM4 decreased with increasing concentrations of free S-methyl-DM4. Points represent the mean of samples in triplicate with standard deviations depicted by the error bars. The two lead clones, DMFH1 and DMOH9, exhibit binding IC50 values to S-methyl-DM4 of 14.9 and 19.4 nM, respectively. **(B)** The lead anti-maytansinoid sdAbs potently inhibit S-methyl-DM4 cytotoxicity. SK-BR-3 cells were incubated with DM4 (30 pM – 1000 nM) with or without co-incubation with 10 μM of purified anti-maytansinoid sdAbs over a 24 h exposure period, following with viability assay to assess cell cytotoxicity. The results were normalized to cells treated with vehicle control and reported as % cell viability. The data was fitted for cytotoxic IC50 values with Hill slope in GraphPad Prism software. Each data point represents the mean of triplicate samples with standard deviations shown with error bars. The IC50 of S-methyl-DM4 applied to SK-BR-3 cells was less than 30 pM. In the presence of purified anti-DM4 sdAbs, DMFH1 and DMOH9, S-methyl-DM4 cytotoxicity was reduced more than 100-fold to IC50s of 3.93 nM and 4.10 nM, respectively.

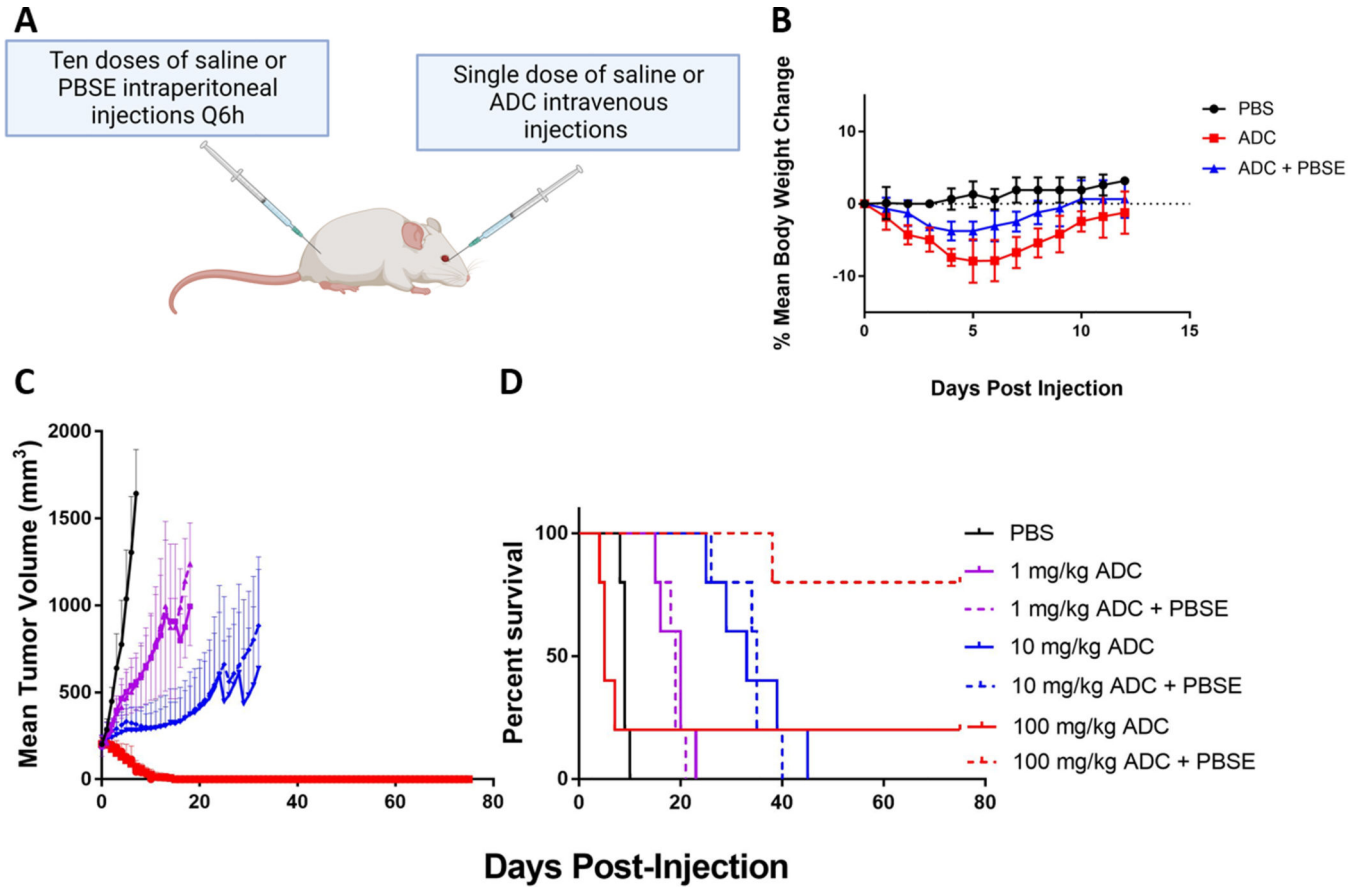

Figure 5. Co-administration of anti-maytansinoid payload-binding selectivity enhancer (PBSE) widens the therapeutic index of 7E7-DM4 ADC.

(A) Dosing schedule of ADC and anti-DM4 PBSE. **(B)** Co-administration of anti-DM4 PBSE reduced ADC-associated body weight loss. Swiss-Webster mice were treated with phosphate-buffered saline (PBS) vehicle control, a single intravenous dose of 55 mg/kg 7E7-DM4 followed by PBS, or 55 mg/kg 7E7-DM4 i.v. with co-dosing with a 10-fold mole-equivalent dose of anti-maytansinoid PBSE via intraperitoneal injections. Percent body weight was calculated with respect to the body weight on the day prior to treatment. Symbols and error bars represent the mean and the standard deviations of the percent body weight (n = 5 per group). Mice administered PBSE with 7E7-ADC had a significantly decreased nadir body weight loss from a mean of 7.9% for ADC+PBS group to 3.8% for ADC+PBSE group (p=0.023). **(C)** *In vivo* efficacy of 7E7-DM4 ADC when administered alone or with anti-maytansinoid sdAb. Mice bearing MOLM-14 AML xenografts were treated with a single IV bolus dose of either PBS (black), 1 mg 7E7-DM4 ADC/kg (purple), 10 mg ADC/kg (blue), or 100 mg ADC/kg (red) followed up with IP co-administration of PBS or 10-fold molar excess of anti-maytansinoid PBSE. The tumor volumes over time for each group are provided with standard deviation error bars. Co-administration of the PBSE did not negatively affect the anti-tumor activity of the ADC. **(D)** Survival curves are shown for each group. Co-administration of the anti-maytansinoid PBSE did not significantly alter survival for mice treated with the ADC at a dose of 1 mg/kg (p=0.49) or 10 mg/kg (p=0.9). In the 100 mg/kg ADC dose groups, excessive morbidity was observed in the mice treated

without PBSE, with an observed median survival time of 5 days. Co-administration of PBSE significantly decreased ADC-associated toxicity and substantially increased survival time.